BIOCHEMISTRY
including biophysical chemistry & molecular biology

Article

pubs.acs.org/biochemistry

Na^+–Substrate Coupling in the Multidrug Antiporter NorM Probed with a Spin-Labeled Substrate

P. Ryan Steed, Richard A. Stein, Smriti Mishra, Michael C. Goodman, and Hassane S. Mchaourab*

Department of Molecular Physiology and Biophysics, Vanderbilt University, Nashville, Tennessee 37232, United States

Supporting Information

ABSTRACT: NorM of the multidrug and toxic compound extrusion (MATE) family of transporters couples the efflux of a broad range of hydrophobic molecules to an inward Na^+ gradient across the cell membrane. Several crystal structures of MATE transporters revealed distinct substrate binding sites leading to differing models of the mechanism of ion-coupled substrate extrusion. In the experiments reported here, we observed that a spin-labeled derivative of daunorubicin, Ruboxyl, is transported by NorM from *Vibrio cholerae*. It is therefore ideal for characterizing mechanistically relevant binding interactions with NorM and directly addressing the coupling of ion and drug binding. Fluorescence and electron paramagnetic resonance experiments revealed that Ruboxyl binds to NorM with micromolar affinity and becomes immobilized upon binding, even in the presence of Na^+. Using double electron–electron resonance spectroscopy, we determined that Ruboxyl binds to a single site on the periplasmic side of the protein. The presence of Na^+ did not translocate the substrate to a second site as previously proposed. These experiments surprisingly show that Na^+ does not affect the affinity or location of the substrate binding site on detergent-solubilized NorM, thus suggesting that additional factors beyond simple mutual exclusivity of binding, such as the presence of a Na^+ gradient across the native membrane, govern Na^+–drug coupling during antiport.

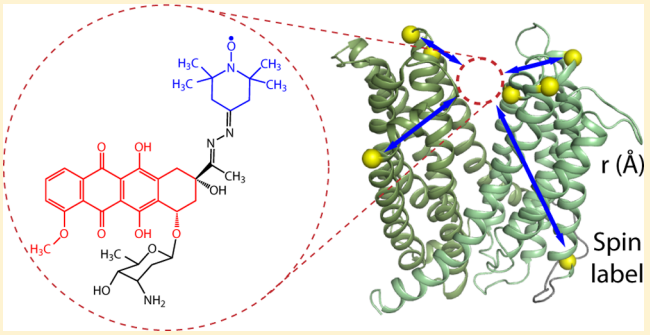

Resistance of bacteria to antibiotics is a significant obstacle to the clinical treatment of infections. One key mechanism of resistance is the active efflux of cytotoxic molecules across the cell membrane, executed by functionally diverse families of transporters with overlapping substrate specificities.[1] The multidrug and toxic compound extrusion (MATE) family encompasses ion–drug antiporters from diverse organisms from bacteria to humans with 12 or 13 transmembrane (TM) helices in a topology distinct from transporters of the major facilitator superfamily.[2,3] Several known MATE transporters, including NorM from *Vibrio cholerae* (*Vc*), couple the efflux of a broad range of compounds to an inward Na^+ gradient.[2,4,5] Biochemical studies of NorM from *Vibrio parahaemolyticus* (77% identical to *Vc*-NorM) identified several conserved, membrane-embedded acidic residues involved in Na^+-coupled transport.[6] He et al.[7] reported a structure of Na^+-coupled *Vc*-NorM in an open-outward state. No substrate was resolved in this moderate-resolution structure, but observation of bound Rb^+ and Cs^+ ions suggested a location of the ion binding site in the proximity of the conserved acidic residues Glu255 on TM7 and Asp371 on TM10. A molecular dynamics simulation of binding of Na^+ to *Vc*-NorM supported this binding location and also predicted transient binding of Na^+ at conserved Asp36 on TM1.[8]

Two sets of crystal structures of MATE transporters have been used to begin to address the location(s) of drug binding (Figure S1 of the Supporting Information). One set of structures of Na^+-coupled NorM from *Neisseria gonorrhea* (*Ng*; 34% identical to *Vc*-NorM) identified ethidium, rhodamine 6G, or tetraphenylphosphonium (TPP) bound to the periplasmic side of the open-outward state (i.e., open to the periplasm) in a site distinct from the Na^+ binding site.[9] Additionally, Tanaka et al.[10] reported structures of a H^+-coupled MATE transporter from *Pyrococcus furiosus* (*Pf*) that revealed norfloxacin bound in a cavity in the middle of the membrane. A pH-dependent obstruction of this cavity, resulting from protonation of conserved Asp41 (Asp36 in *Vc*-NorM), suggested a mechanism of substrate dissociation. The prediction that Na^+ also interacts with this Asp raises the possibility that the same mechanism may operate in Na^+-coupled MATE transporters and that the distinct substrate binding sites observed in *Ng*-NorM and *Pf*-MATE represent ion-dependent steps in drug extrusion.

Fluorescent substrates have long been used to probe substrate binding sites and provide mechanistic insight,[11] but their utility is often limited by various sources of interference, particularly for multidrug transporters in which substrates tend to be hydrophobic and therefore partition into bilayers. This partitioning confounds interpretation of changes in substrate fluorescence as both lipid binding and transporter binding lead to increased fluorescence. Alternatively, electron paramagnetic resonance (EPR) spectroscopy with spin-labeled substrates is virtually free from interference and can reveal the environment of the label, its

Received: March 8, 2013
Revised: July 30, 2013
Published: July 31, 2013

   dx.doi.org/10.1021/bi4008935 | *Biochemistry* 2013, 52, 5790–5799

accessibility, and its distance from other spin-labels. For example, Omote and al-Shawi[12] used spin-labeled verapamil to measure binding to human P-glycoprotein and active uptake of this substrate into proteoliposomes. More recently, Gaffney et al.[13] mapped the binding site of a spin-labeled lipid in soybean lipoxygenase-1.

In this study, we use a spin-labeled derivative of daunorubicin, Ruboxyl, to probe the substrate binding site on Na^+-coupled *Vc*-NorM and its response to Na^+. This compound was developed previously to reduce oxidative side effects of chemotherapeutic daunorubicin treatment.[14] It contains a fluorescent anthracycline moiety and a tetramethylpiperidone nitroxide attached via a hydrazone linker (Figure 1). We show that NorM has a micromolar affinity for Ruboxyl even in the presence of Na^+, and that Ruboxyl binds at a site where the motion of the spin-label moiety is restricted, yielding an immobilized line shape consistent with high-affinity binding. We used double electron−electron resonance (DEER) spectroscopy[15−17] to locate the high-affinity binding site on NorM in the apo and Na^+-bound states. These experiments show that the substrate binds at a single site on *Vc*-NorM and that Na^+ does not induce substrate translocation to a second, distinct site. Furthermore, we establish Ruboxyl as a useful probe for drug binding to address questions about the mechanism of ion-coupled antiport of hydrophobic molecules.

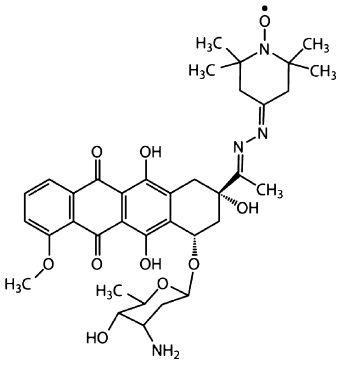

Figure 1. Structure of Ruboxyl.

EXPERIMENTAL PROCEDURES

Test Substrates. Ruboxyl was obtained from Ambinter (Orléans, France). For binding experiments, concentrations of stock solutions of test substrates were determined spectrally as follows: Ruboxyl, daunorubicin, doxorubicin, A_{480} in H_2O, ε = 11500 M^{-1} cm^{-1}; rhodamine 6G, A_{530} in ethanol, ε = 116000 M^{-1} cm^{-1}. Stocks of test substrates were diluted with GF buffer [50 mM HEPES/MES-NaOH and 0.05% β-DDM (pH 7.5)].

Drug Resistance Assay. Drug-sensitive *Escherichia coli* BL21 Δ7 [denoting the deletion of seven genes associated with multidrug resistance (*macAB*, *yojHI*, *acrAB*, *acrEF*, *emrAB*, *emrKY*, and *mdtEF*)] cells[18] were freshly transformed with empty pET19b or pET19b encoding wild-type or mutant NorM with an N-terminal 10-His tag under the control of the inducible T7 promoter. A dense overnight culture of the transformant was used to inoculate 5 mL of LB broth containing 0.1 mg/mL ampicillin and 0.1 mM IPTG. Aliquots (10 μL) of cells in the exponential growth phase (A_{600} = 1.0) were used to inoculate wells of a microplate containing 50% LB broth, 0.1 mg/mL ampicillin, 10 μM IPTG, and 0−34 μM Ruboxyl or doxorubicin. The cell density was measured by A_{600} on a microplate reader after the samples had been grown for 5 h at 37 °C and shaken at 200 rpm. The density was normalized to the density of the wells containing the lowest drug concentration.

Site-Directed Mutagenesis. Wild-type (WT) *norM* in pET19b was used as the template plasmid for construction of Cys-less NorM, which in turn was used as the template for generation of single-Cys substitutions. Substitution mutations were generated using a single-step PCR in which the entire template plasmid was replicated from a single mutagenic primer. The template plasmid was subsequently degraded by *Dpn*I digestion. Plasmids were propagated using XL-1 Blue or DH5α cells, and mutations were confirmed by DNA sequencing.

Expression and Purification of NorM. BL21(DE3) cells were freshly transformed with a pET19b vector encoding WT or mutant NorM with an N-terminal 10-His tag. A transformant colony was used to inoculate a 20 mL LB culture and subsequently 1 L of minimal medium A as previously described.[19] Cultures were incubated while being shaken at 37 °C until they reached an OD_{600} of 1.0, at which time the expression of NorM was induced by the addition of IPTG to a final concentration of 1 mM. The cultures were incubated for an additional 4 h at 30 °C and then harvested and stored overnight at −20 °C. Cell pellets were resuspended in 20 mL of lysis buffer [20 mM Tris-HCl, 20 mM NaCl, 30 mM imidazole, and 5% (v/v) glycerol (pH 8.0)], including 10 mM DTT, and lysed by four passes through an Avestin C3 homogenizer. Cell debris was removed by centrifugation at 9000*g* for 10 min. Membranes were collected from the supernatant by centrifugation at 200000*g* for 1 h. Membrane pellets were resuspended in lysis buffer containing 1% β-dodecyl maltoside (β-DDM) and 0.5 mM DTT and incubated on ice while being stirred for 30−45 min. Insoluble material was cleared by centrifugation at 193000*g* for 30 min. The cleared extract was loaded onto a 4 mL Ni-NTA affinity column equilibrated in Ni buffer [20 mM Tris-HCl, 20 mM NaCl, and 0.05% (w/v) β-DDM (pH 8.0)] at a flow rate of 1.5 mL/min. After being washed with 5 column volumes of Ni buffer containing 30 mM imidazole, NorM was eluted with Ni buffer containing 300 mM imidazole. The eluate was concentrated to 0.5 mL with a spin concentrator (100 kDa, Millipore) and injected onto a Superdex 200 column (GE) equilibrated with GF buffer with or without 20 mM NaCl. Purified NorM was concentrated using a spin concentrator (100 kDa), and the final concentration was determined by A_{280} (ε = 1.075 mg^{-1} cm^{-1}). Purified NorM was stored on ice until it was used within 1 week.

Fluorescence Anisotropy. Dilutions of WT or Cys-less NorM in GF buffer were mixed with a constant concentration of a test substrate in a total volume of 25 μL in a 384-well black microplate and incubated at room temperature for >5 min. The anisotropy of daunorubicin, doxorubicin, and Ruboxyl fluorescence (λ_{ex}, 485 nm; λ_{em}, 595 nm) was measured using a BioTek Synergy H4 microplate reader.

CW-EPR Spectroscopy. Dilutions of Cys-less or Cys-substituted, spin-labeled NorM in GF buffer with or without 20 mM NaCl were mixed with a constant concentration of a test substrate in a total volume of 25 μL and transferred to a glass capillary. Spectra were recorded on a Bruker EMX spectrometer with a microwave power of 10 mW and a modulation amplitude of 1.6 G.

Binding Analysis. Fluorescence anisotropy values and the heights of the high-field resonance lines from CW-EPR spectra were fit with a binding model assuming one site on NorM (P) where affinity for Ruboxyl (L) is described by a dissociation constant, K_D [K_D = ([P][L])/[PL]]. In this system, Ruboxyl

dx.doi.org/10.1021/bi4008935 | *Biochemistry* 2013, 52, 5790−5799

binds to NorM, partitions into DDM micelles, and nonspecifically associates with the NorM−DDM complex. Because it is not practical to deconvolute these binding events, we use [PL] here to describe all Ruboxyl not free in solution. Therefore, K_D values describe an amalgamation of all binding events present in the system. Depletion of unbound NorM and Ruboxyl was accounted for by subtracting NorM and Ruboxyl present in complex (PL) from the total starting concentrations ($[P] = P_{total} - [PL]$; $[L] = L_{total} - [PL]$). Combination of these equations results in a quadratic, which was used to fit the data in Origin 8 (OriginLab Corp., Northampton, MA). The contributions of the signal from bound (I_{bound}) and unbound ($I_{unbound}$) Ruboxyl molecules were related to the total signal (I_{total}) by the equation $I_{total} = f_{bound}I_{bound} + f_{unbound}I_{unbound}$, where f_{bound} and $f_{unbound}$ are the fractions of bound (from [PL]) and unbound (from [L]) Ruboxyl, respectively. $I_{unbound}$ is the fluorescence anisotropy value or height of the high-field line of Ruboxyl with no NorM present. I_{bound} is the y-asymptote of the binding data, dependent on the fit, and is an amalgamation of the signal from all bound species. The K_D from the resulting curve represents an apparent K_D of detergent-solubilized NorM, which includes contributions from the partitioning of Ruboxyl into detergent micelles and nonspecific association (see Results).

DEER Spectroscopy. Dilutions of Cys-less or Cys-substituted, spin-labeled NorM in GF buffer were mixed with the indicated concentrations of test substrates and/or NaCl in a total volume of 10 μL. Glycerol was added to samples to a final concentration of 30% (w/v) as a cryoprotectant. Dipolar time evolution data were collected at 83 K on a Bruker Elexsys E580 spectrometer operating at Q-band frequency (34 GHz) using a standard four-pulse protocol.[20] Raw spin echo decays were analyzed using DeerAnalysis2011[21] and fit using Tikhonov regularization[22] or a single Gaussian model (Figure S2 of the Supporting Information).

Water Accessibility Measurement. Cys-less NorM and Ruboxyl were mixed in a 4:1 ratio and then passed through a spin concentrator (100 kDa) to deplete unbound Ruboxyl. Power saturation curves were measured in a gas-permeable TPX capillary equilibrated in N_2 as previously described.[23] The final concentration of Ni-EDDA was 50 mM.

RESULTS

NorM Transports Ruboxyl. To determine whether Ruboxyl is suitable for probing substrate binding throughout the transport cycle, we tested Ruboxyl transport by *Vc*-NorM using an *in vivo* drug resistance assay. Drug-sensitive *E. coli* BL21 Δ7 cells[18] expressing WT *Vc*-NorM or harboring the empty vector were cultured in the presence of various concentrations of Ruboxyl or doxorubicin, a known substrate of *Vc*-NorM.[5,7] Ruboxyl was toxic to cell growth with an IC_{50} of ∼3 μM compared to an IC_{50} of ∼1 μM for doxorubicin. Expression of *Vc*-NorM, induced by a low concentration of IPTG, allowed cell growth at higher concentrations of Ruboxyl and doxorubicin relative to growth of the nonexpressing cells (Figure 2A). These results suggest that NorM actively extrudes Ruboxyl from the cytoplasm.

Ruboxyl Binds to WT and Cys-less NorM with Micromolar Affinity. To facilitate experiments with Cys-substituted NorM, we used site-directed mutagenesis to generate a NorM construct in which the three endogenous Cys residues at positions 196, 330, and 369 were mutated to Ala, Thr, and Val, respectively. The function of Cys-less NorM was confirmed by measuring resistance to doxorubicin in the drug resistance assay described above (Figure 2A). We determined the binding affinity

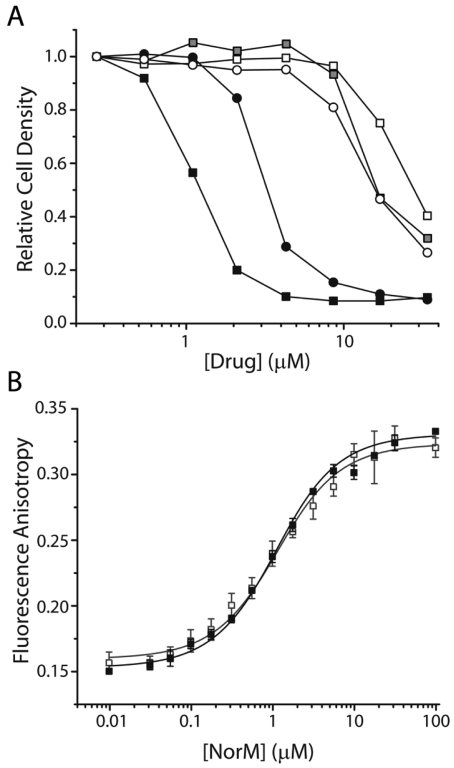

Figure 2. Ruboxyl is a substrate of NorM. (A) The Ruboxyl resistance of drug-sensitive BL21 Δ7 cells was measured using a growth complementation assay. Cells expressing WT NorM (white) or Cys-less NorM (gray) or harboring empty pET19b (black) were cultured in 50% LB containing 0.1 mg/mL ampicillin, 10 μM IPTG to induce NorM expression, and 0−34 μM Ruboxyl (circles) or doxorubicin (squares). The optical density of the cultures relative to the culture with the lowest drug concentration is plotted. (B) *In vitro* binding of Ruboxyl by wild-type (black) or Cys-less (white) NorM was measured by fluorescence anisotropy. Anisotropy values were collected for 25 μL samples containing 0.2 μM Ruboxyl and 0.01−100 μM NorM in GF buffer. The solid lines are nonlinear, least-squares fits assuming a single binding site with an apparent K_D of 0.9 μM (WT) or 1 μM (Cys-less).

of detergent-solubilized Cys-less NorM for Ruboxyl by taking advantage of the fluorescence of the anthracycline moiety (λ_{ex}, 485 nm; λ_{em}, 595 nm). We measured the fluorescence anisotropy of 0.2 μM Ruboxyl at concentrations of NorM from 0.01 to 100 μM. The binding curve was fit with a classic binding model assuming a single binding site characterized by a dissociation constant, K_D. The fit yielded an apparent K_D of 1 μM (Figure 2B). We use "apparent" here because measurement of the intrinsic K_D was hindered by partitioning of Ruboxyl into β-DDM micelles, which appears to be enhanced by nonspecific interactions with NorM in these micelles (see below). Binding affinities of Cys-less NorM for doxorubicin and Ruboxyl were identical to those of the wild type (Figure 2B and Table 1). Therefore, subsequent experiments were conducted with the Cys-less construct.

Ruboxyl Becomes Immobilized upon Binding. Ruboxyl offers the added benefit of detection of binding by the immobilization of the spin-label moiety, evident by changes in the CW-EPR spectral line shape. In GF buffer with 20 mM Na^+ and detergent but no NorM, the EPR line shape of Ruboxyl was characteristic of fast motion, as expected for free tumbling in solution (Figure 3A, black). Incubation of Ruboxyl with NorM resulted in a multicomponent spectrum (Figure 3A, red). The

dx.doi.org/10.1021/bi4008935 | *Biochemistry* 2013, 52, 5790−5799

Table 1. Binding Affinities of Wild-Type and Cys-less NorM

	apparent K_D[a] (μM)		
NorM	doxorubicin	daunorubicin	Ruboxyl
wild type	0.6	nd[b]	0.9
Cys-less	0.6	2.5	1.0

[a]Calculated from a nonlinear, least-squares fit of fluorescence anisotropy data (see Experimental Procedures). [b]Not determined.

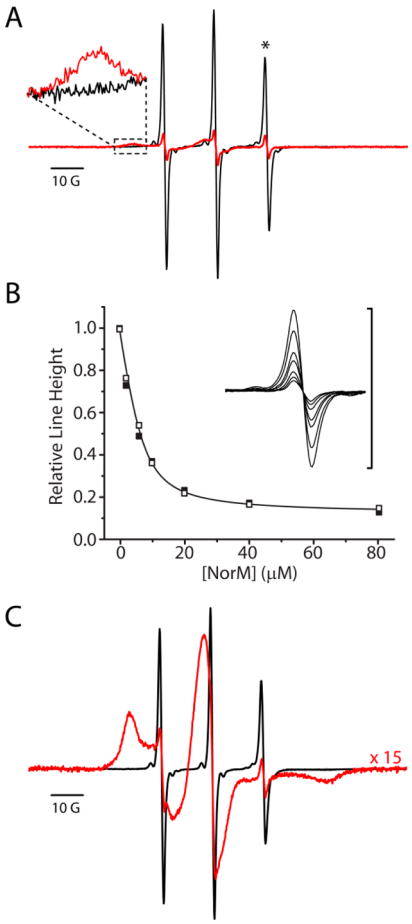

Figure 3. Immobilization of bound Ruboxyl. CW-EPR spectra were recorded for 25 μL samples containing 7 μM Ruboxyl and 0−80 μM NorM in GF buffer. (A) The spectrum of free Ruboxyl (black) shows sharp lines characteristic of a mobile nitroxide. The high-field resonance line is marked with an asterisk. The spectrum of Ruboxyl with 80 μM NorM (red) shows features of an immobilized nitroxide and diminished intensity of sharp resonance lines. The inset shows the broadened low-field line. (B) The relative height of the high-field resonance line (inset) decreases with increasing NorM concentrations. Line heights were normalized to that of free Ruboxyl. Similar binding was observed in the presence (■) or absence (□) of 20 mM NaCl. A nonlinear, least-squares fit of the Na^+-free condition assuming a single binding site with an apparent K_D of 1.8 μM (—) fits well with both binding curves. The fit of the Na^+ condition (not shown) is superimposable and has an apparent K_D of 1.5 μM. (C) Spectrum of 80 μM free Ruboxyl (black) compared to the spectrum of 80 μM Ruboxyl in the presence of 440 μM NorM (red). The bound spectrum was multiplied by 15 to show the details of the line shape.

most mobile component, characterized by sharp resonance lines, is similar to that observed in buffer without NorM and arises from the fraction of Ruboxyl that remained unbound in solution. The least mobile component, characterized by the outer extrema (inset in Figure 3A), is consistent with a loss of isotropic motion and arises from Ruboxyl bound to NorM in a sterically restrictive environment. To quantitate binding, we measured the height of the high-field resonance line (star in Figure 3A) at increasing concentrations of NorM. The intensity of this line has little contribution from the spectrum of bound Ruboxyl, which is significantly broader. Therefore, this line best represents the fraction of unbound Ruboxyl. The binding curve, determined from the decrease in the peak height of the high-field resonance line (Figure 3B) and calculated as described in Experimental Procedures, indicated an apparent K_D of 1.5 μM, consistent with the value determined by fluorescence anisotropy. We observed a similar binding curve for wild-type NorM (data not shown).

Even at saturating concentrations of NorM (11-fold molar excess over Ruboxyl), a small fraction of the fast, free signal remained in the CW-EPR spectrum (~12% from the experiment in Figure 3A,B). This signal could arise from free spin-label hydrolyzed from Ruboxyl or a fraction of Ruboxyl that partitions into detergent micelles and is not accessible to NorM. We repeated several points of the binding curve using 5-fold higher concentrations of Ruboxyl and NorM while holding the β-DDM concentration constant. In this experiment (Figure 3C), the fraction of spins remaining in the fast component in the presence of excess NorM was reduced to approximately 1.5%, suggesting that these spins remain mobile because of the partitioning of Ruboxyl molecules into β-DDM micelles rather than hydrolysis of the label. The concentration of spins contributing to the fast component of the spectrum (1−2 μM) was on the order of the concentration of empty β-DDM micelles [0.05% (w/v) β-DDM = 7.0−8.8 μM]. This calculation assumes an aggregation number of 110−140,[24] though Anatrace reports values from 78 to 149.

NorM Substrates, but Not Na^+, Displace Ruboxyl at the High-Affinity Site. To determine whether Ruboxyl binds to a site shared by other known substrates, we added NorM to a mixture of Ruboxyl and an excess of doxorubicin, daunorubicin, or rhodamine 6G to compete for the Ruboxyl binding site in the presence of 20 mM NaCl. Ruboxyl binding was gauged by the height of the high-field resonance line. Figure 4A shows that approximately half of the Ruboxyl molecules bound NorM even in the presence of a 50-fold excess of competitor. The CW-EPR line shape of Ruboxyl in the presence of NorM and excess doxorubicin (Figure 4B) showed a reduction of the immobilized component, indicating that competitors block the binding of Ruboxyl to the high-affinity site. This competition suggested that approximately half of Ruboxyl molecules bind to the drug binding site shared with known substrates, but that additional Ruboxyl molecules bind elsewhere on NorM (see below). We observed a similar degree of competition in the absence of Na^+ (data not shown).

Because NorM is a Na^+-coupled transporter, we measured the effect of Na^+ on Ruboxyl binding using the EPR line shape by preparing Cys-less NorM in Na^+-free buffer. Ruboxyl binding, as measured by the height of the high-field resonance line, was nearly identical to binding in the presence of 20 mM Na^+ and indicated an apparent K_D of 1.8 μM (Figure 3B). Furthermore, inclusion of Na^+ in a mixture of Ruboxyl and NorM did not prevent Ruboxyl binding (Figure 4C).

Additional Ruboxyl Molecules Bind Nonspecifically. The inability of competitors to completely prevent Ruboxyl binding suggested that Ruboxyl molecules may also bind NorM nonspecifically. The line shape of the population of Ruboxyl molecules that binds to NorM in the presence of doxorubicin was more restricted than that of free Ruboxyl but more mobile than

dx.doi.org/10.1021/bi4008935 | Biochemistry 2013, 52, 5790−5799

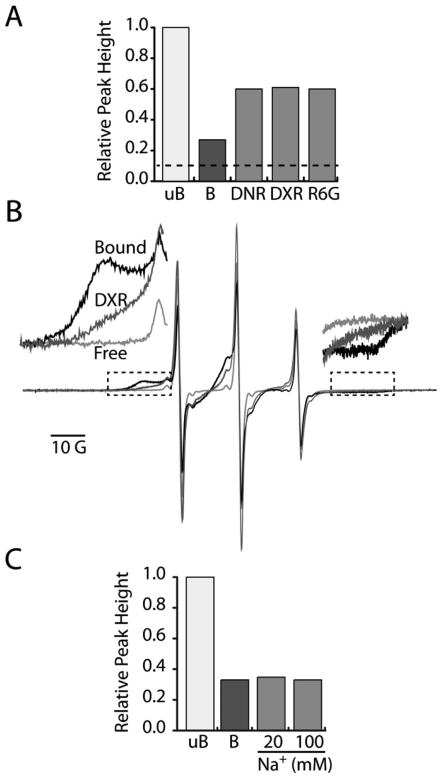

Figure 4. Competition for the substrate binding site. (A) Peak height of the high-field resonance line of 7 μM Ruboxyl in GF buffer with 20 mM NaCl (uB) compared to peak heights of Ruboxyl bound to 10 μM NorM without competitor (B) or in the presence of 350 μM daunorubicin (DNR), doxorubicin (DXR), or rhodamine 6G (R6G). Peak heights were normalized to that of free Ruboxyl. The dashed line indicates the fraction of the signal resulting from detergent-bound Ruboxyl. (B) CW-EPR spectra of bound Ruboxyl (110 μM NorM and 80 μM Ruboxyl) in the presence (dark gray) or absence (black) of 2.8 mM doxorubicin. The spectrum of 80 μM Ruboxyl without NorM is plotted (30% of full signal) in light gray for line shape comparison. Inset spectral details show the disappearance of the immobilized component in the presence of doxorubicin. (C) Peak height of the high-field resonance line of 7 μM Ruboxyl in GF buffer (uB) compared to peak heights of Ruboxyl bound to 10 μM NorM without Na^+ (B) or in the presence of 20 or 100 mM NaCl.

that of bound Ruboxyl, consistent with lower-affinity binding or nonspecific association (Figure 4B). We hypothesize that this component results from the partitioning of Ruboxyl molecules into detergent micelles containing NorM, possibly interacting with its surface.

Nonspecific binding of Ruboxyl to detergent and/or NorM could interfere with experiments to localize the substrate binding site. Therefore, we determined conditions to select for Ruboxyl binding in the specific, competitor-sensitive site. When more than one Ruboxyl molecule is bound to the NorM–DDM complex simultaneously, it should be possible to detect a dipolar interaction between the two nitroxide moieties. The CW-EPR spectra recorded during the experiments shown in Figures 3 and 4 did not indicate short-range dipolar coupling, suggesting that the binding sites must place the multiple spin-label moieties >20 Å apart. Therefore, we used DEER spectroscopy to detect a longer-range dipolar interaction. With a 6-fold molar excess of NorM, only the primary, high-affinity binding site on NorM should be occupied by Ruboxyl. At the other end of the range, a 3-fold excess of Ruboxyl should occupy every available site on NorM and in complex with detergent. Consistent with this model, the relative depth of modulation of the echo decay, which is an indicator of the fraction of interacting spins at a constant total concentration of Ruboxyl, increased with decreasing amounts of NorM (Figure 5A). This result demonstrates that

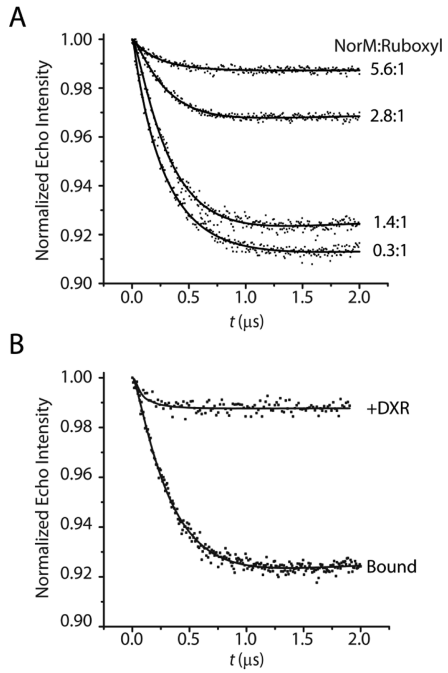

Figure 5. Binding of additional Ruboxyl molecule(s) is nonspecific. (A) DEER decays are shown for samples containing 80 μM Ruboxyl and 20–440 μM NorM (the molar ratio of NorM to Ruboxyl is noted) in GF buffer with 20 mM NaCl. (B) DEER decays are shown for bound Ruboxyl (110 μM NorM and 80 μM Ruboxyl) in the absence or presence of 2.8 mM doxorubicin.

excess Ruboxyl promoted binding to nonspecific sites in the NorM–micelle complex. The depth of modulation appeared to approach a maximum with a 3-fold excess of Ruboxyl, suggesting that two or three Ruboxyl molecules bind on the NorM–DDM complex. No echo decay was observed with Ruboxyl in DDM micelles when NorM was absent (data not shown), indicating that one of the sites is specific to NorM, presumably the high-affinity site characterized by the immobilized line shape. The shapes of the spin echo decays at each NorM:Ruboxyl ratio were consistent with broad distributions of distances from 20 to 60 Å reflecting the high degree of disorder in at least one of the binding sites. To confirm that the dipolar interaction involved the Ruboxyl molecules occupying the high-affinity site, we measured the echo decay of a 1.4:1 NorM:Ruboxyl ratio in the presence of excess doxorubicin. The competitor reduced the level of dipolar interaction to almost undetectable levels (Figure 5B), which we interpret as the competitor excluding Ruboxyl from the high-affinity site.

High-Affinity Ruboxyl Binding Occurs at a Single Site. Because Ruboxyl bound at the high-affinity site is highly ordered, as evidenced by the immobilized spectral line shape, it was possible to measure distances between bound Ruboxyl and single spin-labeled sites on NorM. For this purpose, we introduced single spin-labels at positions 44, 54, 125, 267, 269, and 338 on the periplasmic side of *Vc*-NorM and at position 216 on the cytoplasmic side (Figure 6A). These positions were selected on the basis of their locations at the ends of helices surrounding the

dx.doi.org/10.1021/bi4008935 | *Biochemistry* 2013, 52, 5790–5799

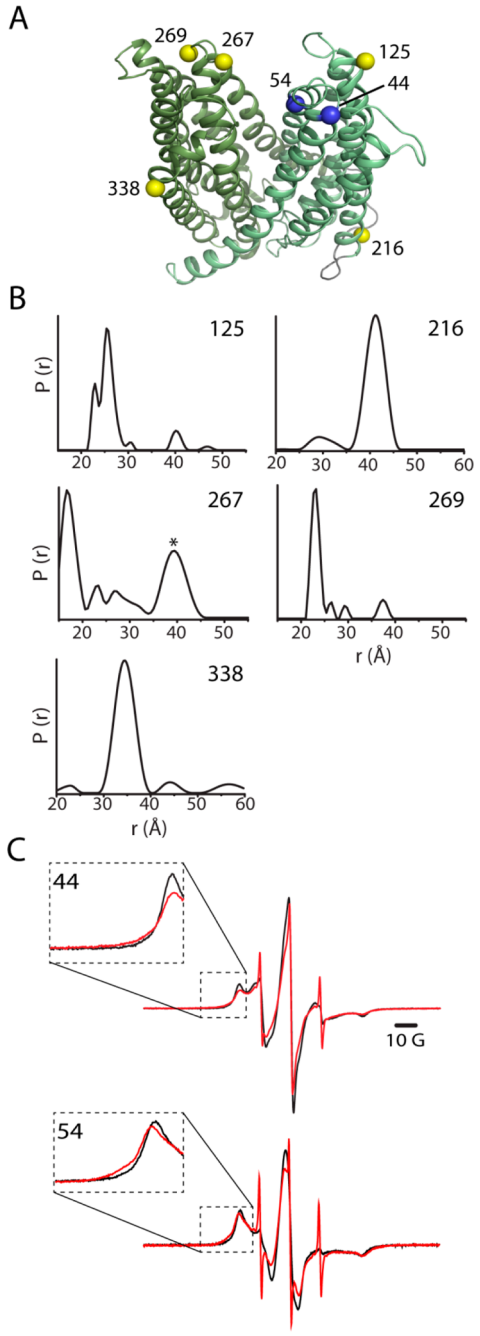

Figure 6. Measurements of distances to bound Ruboxyl. (A) The positions of spin-labels used for distance measurements with DEER (yellow) or CW-EPR (blue) are shown as spheres on the structure of *Vc*-NorM (PDB entry 3MKT). (B) Distributions of distances (r) between Ruboxyl and spin-labels at positions 125, 216, 267, 269, and 338. Samples were prepared with NorM and Ruboxyl maintaining a NorM:Ruboxyl molar ratio of 3.75:1. The peak marked with as asterisk in the distance distribution from position 267 arose from aggregation, which was evident in the DEER decay as a long, poorly defined component (Figure S2 of the Supporting Information). (C) CW-EPR spectra in the presence (red) or absence (black) of Ruboxyl are shown for labels at positions 44 and 54. Spectral details show broadening of the low-field resonance line.

putative drug binding cleft. We measured the distances between each site and bound Ruboxyl in the absence of Na^+ using DEER spectroscopy. Experiments were conducted with a 4-fold excess of NorM to select for Ruboxyl binding to the high-affinity site and to reduce the level of nonspecific binding. For Ruboxyl-bound NorM labeled at positions 125, 216, 267, 269, and 338, we observed oscillating spin echo decays (Figure S2 of the Supporting Information) indicative of well-defined distributions of distances centered at 25, 42, 17, 23, and 34 Å, respectively (Figure 6B). The narrow distance distributions are consistent with Ruboxyl binding at a single, specific site. We confirmed that the dipolar interaction between Ruboxyl and the label at position 216 arose from Ruboxyl bound in the high-affinity site by measuring the spin echo decay in the presence of excess doxorubicin. The presence of competitor greatly attenuated the oscillation in the spin echo decay by excluding Ruboxyl from the high-affinity site (Figure S3 of the Supporting Information). Additionally, we observed dipolar coupling in the CW-EPR spectra of Ruboxyl-bound NorM labeled at positions 44 and 54 indicated by broadening of the low-field resonance line (Figure 6C).

Location of the Ruboxyl Binding Site. Distance distributions from DEER experiments were used to locate the position of the nitroxide moiety of Ruboxyl bound to NorM using the crystal structures of NorM as a scaffold. To facilitate this triangulation, we first modeled the spin-label rotamers at the seven labeled sites on structural models derived from the crystal structures of cation-bound *Vc*-NorM (PDB entry 3MKT) and rhodamine-bound *Ng*-NorM (PDB entry 4HUN) using MMM.[25] This program generates rotamers of the spin-label side chain that are sterically compatible with the modeled protein structure at the labeled site. A potential position of the Ruboxyl nitroxide was triangulated using distances from the top 26 rotamers for spin-labels at positions 125, 216, 267, 269, and 338. To accommodate potential errors in the structural model and rotamer placement, we conducted fitting with all combinations of three distances (to reduce the weight of any one spin-label position in the fitted position of Ruboxyl) and allowed the position of the Ruboxyl nitroxide to deviate from the measured DEER distance by ~4 Å. This fitting procedure yielded up to 17576 potential positions from each of the 10 sets of spin-label combinations. To cull the number of potential positions, we eliminated those positions incompatible with short-range dipolar coupling interactions with spin-labels at positions 44 and 54 (i.e., 10−27 Å from the C_α position of these residues). To further restrict the placement of potential Ruboxyl positions, we determined the exposure of the Ruboxyl nitroxide to water by measuring the frequency of collisions with Ni-EDDA, a water-soluble paramagnetic relaxing agent. Low to moderate accessibility to Ni-EDDA (Π = 0.45) allowed us to restrict potential positions to those inside the binding cleft, which is also consistent with the immobilized EPR line shape.

This constrained triangulation procedure using the structure of *Vc*-NorM (PDB entry 3MKT) generated a band of potential Ruboxyl nitroxide positions on the periplasmic side of the open cleft running from TM 3 along the C-terminal half of the cleft and ending at TM 8 (Figure 7A). Notably, there is a confluence of points between TM 2 and TM 7 consistent with all combinations of distances (arrow in Figure 7A). Because this method depends on the reliability of the backbone assignments in the crystal structure, we also conducted the triangulation procedure using the higher-resolution, substrate-bound structure of *Ng*-NorM (PDB entry 4HUN). Equivalent amino acid positions between *Vc*-NorM and *Ng*-NorM were derived from the alignment reported by Lu et al.[9] Significantly, this alignment places residue 125 in the loop between TM 3 and TM 4 rather than on TM 4, thus displacing the position of the α-carbon by 15 Å (compare

dx.doi.org/10.1021/bi4008935 | *Biochemistry* 2013, 52, 5790−5799

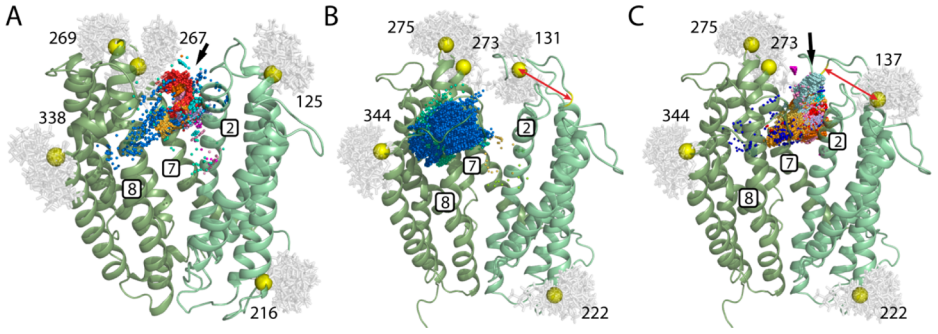

Figure 7. Location of bound Ruboxyl. Ribbon representations of the crystal structures of *Vc*-NorM (A) and *Ng*-NorM (B and C) are shown from a periplasmic perspective. TM 1 has been omitted for the sake of clarity. Positions of spin-labels are shown as yellow spheres denoting the C_α position surrounded by the cloud of most likely rotamers of the spin-label side chain generated by MMM. Possible positions of the Ruboxyl nitroxide are shown as small spheres, where coloring differentiates positions derived from triangulation using different sets of three distances. (A) Using the crystal structure of *Vc*-NorM as a scaffold resulted in a band of potential Ruboxyl nitroxide positions on the periplasmic side of the cleft with a confluence of points (arrow) lying between TM 2 and TM 7. (B) Using the crystal structure of *Ng*-NorM and the 3−4 loop position of *Vc*-NorM residue 125 (*Ng*-NorM residue 131) results in nitroxide positions surrounding TM 8. Combinations of distances that do not include position 125 are omitted. (C) Using the crystal structure of *Ng*-NorM and the TM 4 position of *Vc*-NorM residue 125 (*Ng*-NorM residue 137) results in a confluence of potential Ruboxyl nitroxide positions (arrow) similar to that seen with *Vc*-NorM (panel A). The red arrows in panels B and C indicate the difference between the placement of the sequence equivalent or the structural equivalent of *Vc*-NorM residue 125.

panels B and C of Figure 7). For this reason, we used a set of 16 combinations of three distances, which included distances from either the end of TM 4, consistent with structural position 125 in *Vc*-NorM (137 in *Ng*-NorM), or the 3−4 loop, the equivalent position in *Ng*-NorM (131) based on the sequence alignment. A similar band of potential Ruboxyl nitroxide positions in the periplasmic cleft was generated. Measurement from the 3−4 loop position of 125 places the Ruboxyl nitroxide in the cleft near the periplasmic end of TM 8 (Figure 7B), but this location is not consistent with all distances. When the distance is measured from position 125 of TM 4, a confluence of points appeared between TM 2 and TM 7 similar to the cluster generated on the *Vc*-NorM scaffold (arrow in Figure 7C). This cluster of potential positions of the Ruboxyl nitroxide is consistent with the placement of the high-affinity Ruboxyl binding site in the periplasmic cleft.

Na^+ Does Not Alter the Location of Ruboxyl Binding. To address the possibility that Na^+ binding drives substrate translocation to a distinct binding site, we measured the distances from Ruboxyl to the spin-labeled sites mentioned above in the presence of 70 mM NaCl. For Ruboxyl-bound NorM labeled at positions 125, 216, 267, 269, and 338, we observed oscillating spin echo decays resulting in distance distributions similar to those observed under Na^+-free conditions (Figure 8A). For Ruboxyl-bound NorM labeled at positions 44 and 54, broadening of the CW-EPR line shape due to dipolar coupling was similar to broadening observed under Na^+-free conditions (Figure 8B). These results indicate that the position of the nitroxide of Ruboxyl is not altered by the presence of Na^+.

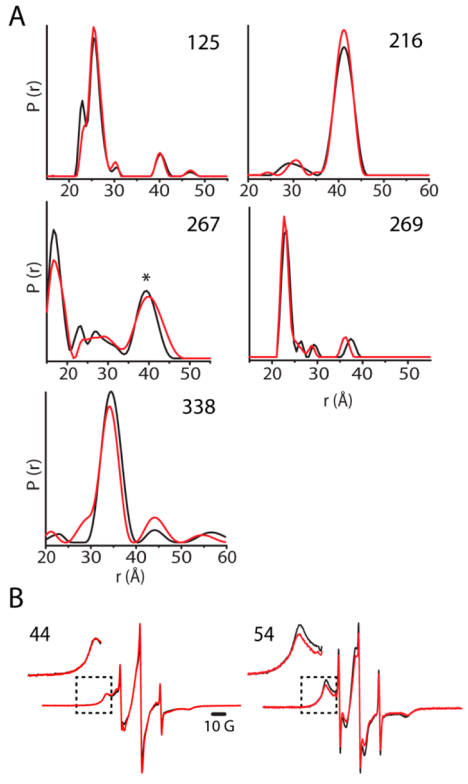

Figure 8. Effect of Na^+ on measured distances to bound Ruboxyl. (A) Distributions of distances (r) between Ruboxyl and spin-labels at positions 125, 216, 267, 269, and 338. Samples were prepared in the presence (red) or absence (black) of 70 mM NaCl with NorM and Ruboxyl maintaining a NorM:Ruboxyl molar ratio of 3.75:1. (B) CW-EPR spectra of Ruboxyl bound to NorM spin-labeled at position 44 or 54 in the presence (red) or absence (black) or 70 mM NaCl. Spectral details show the low-field resonance line. The peak marked with an asterisk in the distance distribution from position 267 arose from aggregation, which was evident in the DEER decay as a long, poorly defined component (Figure S2 of the Supporting Information).

DISCUSSION

Current models of antiport by MATE family transporters based on the crystal structures of *Vc*-NorM,[7] *Ng*-NorM,[9] and *Pf*-MATE[10] propose a conformational change, induced by binding of the coupling ion, that results in reduced binding affinity for substrates (Figure S1 of the Supporting Information). Additionally, the substrate binding site observed in *Ng*-NorM differs from that observed in *Pf*-MATE, raising the possibility of ion-driven translocation of substrate through multiple sites during transport. In this study, we have identified a spin-labeled substrate of *Vc*-NorM, Ruboxyl, and used EPR spectroscopy to monitor this substrate in its binding site to address questions of drug binding and translocation during ion-coupled antiport by a MATE transporter. We found that Ruboxyl binds to a single, periplasmic site and that neither the affinity nor the location of this site is

dx.doi.org/10.1021/bi4008935 | *Biochemistry* 2013, 52, 5790−5799

altered by Na^+. Independence of substrate and Na^+ binding conflicts with the classical model of antiport in which binding of substrate and coupling ion is mutually exclusive and thus raises questions about the mechanism of coupling in NorM during drug antiport.

Ruboxyl is a spin-labeled derivative of daunorubicin, a known substrate of NorM.[5] We show that Ruboxyl is toxic to cells and that expression of *Vc*-NorM confers resistance to this toxicity (Figure 2A), indicating that *Vc*-NorM transports Ruboxyl. Furthermore, the micromolar affinity of Ruboxyl is equivalent to affinities reported for binding of drug to *Vc*-NorM and its homologues.[7,26] Therefore, the interaction of Ruboxyl that we have characterized here is relevant to the transport mechanism and likely not unique to this molecule. We foresee the further utilization of Ruboxyl to probe the substrate binding site(s) on MATE transporters and the many other multidrug transporters that transport anthracyclines.[2,11,27−30]

The EPR data indicated that the apparent binding affinity for Ruboxyl has contributions from multiple binding modes. Most interesting and informative, binding of Ruboxyl to a high-affinity site on *Vc*-NorM is evident in the appearance of an immobilized component in the EPR line shape and marked reduction of this component in the presence of an excess of known *Vc*-NorM substrates acting as competitors. This immobilized population likely represents the Ruboxyl molecules bound with higher affinity to the native substrate binding site. In contrast, nonspecifically bound Ruboxyl did not respond to the presence of competitors and had a more mobile EPR line shape reflecting disorder of the bound molecule. We hypothesize that Ruboxyl molecules bound to *Vc*-NorM with a high degree of disorder are nonspecifically associated with detergent molecules in complex with solubilized *Vc*-NorM. Given the convolution of binding modes, we report only the apparent K_D for binding of Ruboxyl to *Vc*-NorM in β-DDM micelles. Earlier characterizations of NorM that used anisotropy as a measure for binding of doxorubicin[7] or rhodamine 6G[26] in the presence of detergent have likely also reported an apparent K_D with contributions from multiple binding modes, and this convolution should be expected in all measurements of binding of a hydrophobic ligand to a detergent-solubilized receptor.

In the crystal structures of *Ng*-NorM bound to TPP, ethidium, or rhodamine 6G, the substrates bind to the same location on the periplasmic side of the cleft between the two halves of *Ng*-NorM in an apparently open-outward state. We have used distances between bound Ruboxyl and seven spin-labeled sites on NorM, determined by DEER and CW-EPR spectroscopy, to triangulate the high-affinity site of Ruboxyl binding using the crystal structures of *Vc*-NorM and *Ng*-NorM as a scaffold. These two structural models are very similar, but differences in helical register became apparent when label positions were chosen for distance measurements. The most significant discrepancy between the structures was the position of residue 125, which sits on the top of TM 4 in *Vc*-NorM but is placed in the extended 3−4 loop of *Ng*-NorM by sequence alignment. Therefore, we compared the triangulation results from both structures to take advantage of the higher-resolution and substrate-bound state of the *Ng*-NorM structure. The results of the triangulation procedure placed the position of the nitroxide of bound Ruboxyl at the edge of the periplasmic cleft near TM7. This position is consistent with the location occupied by substrates in the crystal structures of *Ng*-NorM and is in the proximity of the hairpin formed by TM 7 and TM 8, which is proposed to move in response to ion and/or substrate binding.[9] Because the linkage between the bulk of Ruboxyl and the nitroxide is flexible, we are unable to establish the orientation of the Ruboxyl in the binding site. Even so, the triangulated position of Ruboxyl is not consistent with the occupancy of a more cytoplasmic site in the cleft as observed in the crystal structure of norfloxacin-bound *Pf*-MATE.[10] The data presented here indicate a single binding site and offer no evidence of ion-induced translocation of the substrate between multiple sites. Indeed, no effect of the coupling Na^+ ion was observed in our experiments.

The absence of an effect of Na^+ on Ruboxyl binding is surprising given that drug antiport by VcmA (a 99% identical orthologue of *Vc*-NorM) as well as *Vp*-NorM and *Ng*-NorM has been shown to be Na^+-coupled.[4,5,26] In the classical paradigm of ion-coupled antiport, transporters alternate between an inward-facing state with high affinity for substrate and low affinity for ion and an outward-facing state in which the reverse is true. Mutually exclusive binding of substrate to the inward-facing state and ion to the outward-facing state induces the opposite state. The data presented here show that the location and apparent affinity of the Ruboxyl binding site are not dependent on the presence of Na^+ under these conditions. This observation is not consistent with mutually exclusive binding of substrate and coupling ion. One possible explanation is that we did not use a sufficient concentration of Na^+ to elicit a structural response from NorM that would lead to substrate release. However, our preliminary observations indicate that 70 mM Na^+ is enough to induce structural changes in NorM (P. R. Steed and H. S. Mchaourab, unpublished observations). Although mutually exclusive binding has been shown for H^+-coupled drug antiporters,[31,32] no experiments have shown substrate-induced Na^+ release or vice versa. In the only other direct study of substrate binding to a MATE transporter, Long et al.[26] also failed to observe a strong effect of Na^+ on binding of rhodamine 6G to *Ng*-NorM, showing that varying the Na^+ concentration from 0 to 100 mM shifted the K_D by only 2.5 μM. The absence of a Na^+ effect observed by these methods may indicate that the classical paradigm of antiport is an oversimplification, at least in the case of NorM. An emerging body of evidence suggests that a transport cycle, rather than proceeding by complete shifts between distinct states, involves transporters adopting multiple states in equilibrium.[33−35] Ions and substrates modulate the fractional occupancy of these states rather than shifting one to another. In this case, the effect of Na^+ during transport may be dependent on the presence of a Na^+ concentration gradient across the membrane such that our measurements of substrate affinity in a detergent-solubilized system at thermodynamic equilibrium may miss any effect of Na^+. Answering the question of how Na^+ causes the substrate to dissociate will require measurements of substrate and ion binding in the presence of a gradient or measurement of trapped states in the transport cycle along with definition of how ions and substrates modulate the equilibrium among these states.

■ ASSOCIATED CONTENT

Ⓢ Supporting Information

An additional introductory figure, raw DEER decays, and details of DEER data analysis. This material is available free of charge via the Internet at http://pubs.acs.org.

■ AUTHOR INFORMATION

Corresponding Author

*Department of Molecular Physiology and Biophysics, 741 Light Hall, 2215 Garland Ave., Nashville, TN 37232. Telephone: (615) 322-3307. E-mail: hassane.mchaourab@vanderbilt.edu.

Funding

This work was supported by National Institutes of Health Grants F32 GM100569 to P.R.S. and R01 GM077659 to H.S.M.

Notes

The authors declare no competing financial interest.

■ ACKNOWLEDGMENTS

We thank Geoffrey Chang for providing the NorM expression plasmid, Hiroyasu Yamanaka for providing the BL21 Δ7 strain, Ping Zou for assistance with the Cys-less NorM construct, and Cesar Luna-Chavez for the initiation of preliminary experiments with spin-labeled daunorubicin obtained from Natalya Rapoport. We also thank Elizabeth Nguyen for helpful discussions of Ruboxyl binding as well as Kelli Kazmier and Brandy Verhalen for critically reading the manuscript.

■ ABBREVIATIONS

CW, continuous wave; β-DDM, β-dodecyl maltoside; DTT, dithiothreitol; DEER, double electron−electron resonance; EDDA, ethylenediamine-*N*,*N*′-diacetic acid; EPR, electron paramagnetic resonance; HEPES, 4-(2-hydroxyethyl)-1-piperazineethanesulfonic acid; IPTG, isopropyl β-D-1-thiogalactopyranoside; MATE, multidrug and toxic compound extrusion; MES, 2-(*N*-morpholino)ethanesulfonic acid; *Ng*, *N. gonorrhea*; NTA, nitrilotriacetic acid; PCR, polymerase chain reaction; PDB, Protein Data Bank; *Pf*, *P. furiosus*; TM, transmembrane; TPP, tetraphenylphosphonium; *Vc*, *V. cholerae*; *Vp*, *V. parahaemolyticus*.

■ REFERENCES

(1) Higgins, C. F. (2007) Multiple molecular mechanisms for multidrug resistance transporters. *Nature 446*, 749−757.

(2) Kuroda, T., and Tsuchiya, T. (2009) Multidrug efflux transporters in the MATE family. *Biochim. Biophys. Acta 1794*, 763−768.

(3) Omote, H., Hiasa, M., Matsumoto, T., Otsuka, M., and Moriyama, Y. (2006) The MATE proteins as fundamental transporters of metabolic and xenobiotic organic cations. *Trends Pharmacol. Sci. 27*, 587−593.

(4) Morita, Y., Kataoka, A., Shiota, S., Mizushima, T., and Tsuchiya, T. (2000) NorM of *Vibrio parahaemolyticus* is an Na^+-driven multidrug efflux pump. *J. Bacteriol. 182*, 6694−6697.

(5) Huda, M. N., Morita, Y., Kuroda, T., Mizushima, T., and Tsuchiya, T. (2001) Na^+-driven multidrug efflux pump VcmA from *Vibrio cholerae* non-O1, a non-halophilic bacterium. *FEMS Microbiol. Lett. 203*, 235−239.

(6) Otsuka, M., Yasuda, M., Morita, Y., Otsuka, C., Tsuchiya, T., Omote, H., and Moriyama, Y. (2005) Identification of essential amino acid residues of the NorM Na^+/multidrug antiporter in *Vibrio parahaemolyticus*. *J. Bacteriol. 187*, 1552−1558.

(7) He, X., Szewczyk, P., Karyakin, A., Evin, M., Hong, W.-X., Zhang, Q., and Chang, G. (2010) Structure of a cation-bound multidrug and toxic compound extrusion transporter. *Nature 467*, 991−994.

(8) Vanni, S., Campomanes, P., Marcia, M., and Rothlisberger, U. (2012) Ion binding and internal hydration in the multidrug resistance secondary active transporter NorM investigated by molecular dynamics simulations. *Biochemistry 51*, 1281−1287.

(9) Lu, M., Symersky, J., Radchenko, M., Koide, A., Guo, Y., Nie, R., and Koide, S. (2013) Structures of a Na^+-coupled, substrate-bound MATE multidrug transporter. *Proc. Natl. Acad. Sci. U.S.A. 110*, 2099−2104.

(10) Tanaka, Y., Hipolito, C. J., Maturana, A. D., Ito, K., Kuroda, T., Higuchi, T., Katoh, T., Kato, H. E., Hattori, M., Kumazaki, K., Tsukazaki, T., Ishitani, R., Suga, H., and Nureki, O. (2013) Structural basis for the drug extrusion mechanism by a MATE multidrug transporter. *Nature 496*, 247−251.

(11) Smriti, Zou, P., and Mchaourab, H. S. (2009) Mapping daunorubicin-binding sites in the ATP-binding cassette transporter MsbA using site-specific quenching by spin labels. *J. Biol. Chem. 284*, 13904−13913.

(12) Omote, H., and Al-Shawi, M. K. (2002) A novel electron paramagnetic resonance approach to determine the mechanism of drug transport by P-glycoprotein. *J. Biol. Chem. 277*, 45688−45694.

(13) Gaffney, B. J., Bradshaw, M. D., Frausto, S. D., Wu, F., Freed, J. H., and Borbat, P. (2012) Locating a lipid at the portal to the lipoxygenase active site. *Biophys. J. 103*, 2134−2144.

(14) Emanuel, N., Konovalova, N., Povarov, L., Shapiro, A., Dyachkovskaya, R., Suskina, V., and Denisova, L. (1982) 13-(1-Oxyl-2, 2, 6, 6-tetramethylpiperylidenyl-4) hydrazone rubomycin hydrochloride with a paramagnetic center and a method of producing same. U.S. Patent 4,332,934.

(15) Jeschke, G., and Polyhach, Y. (2007) Distance measurements on spin-labelled biomacromolecules by pulsed electron paramagnetic resonance. *Phys. Chem. Chem. Phys. 9*, 1895−1910.

(16) Borbat, P. P., Surendhran, K., Bortolus, M., Zou, P., Freed, J. H., and Mchaourab, H. S. (2007) Conformational motion of the ABC transporter MsbA induced by ATP hydrolysis. *PLoS Biol. 5*, e271.

(17) Mchaourab, H. S., Steed, P. R., and Kazmier, K. (2011) Toward the Fourth Dimension of Membrane Protein Structure: Insight into Dynamics from Spin-Labeling EPR Spectroscopy. *Structure 19*, 1549−1561.

(18) Yamanaka, H., Kobayashi, H., Takahashi, E., and Okamoto, K. (2008) MacAB is involved in the secretion of *Escherichia coli* heat-stable enterotoxin II. *J. Bacteriol. 190*, 7693−7698.

(19) Koteiche, H. A., Reeves, M. D., and Mchaourab, H. S. (2003) Structure of the substrate binding pocket of the multidrug transporter EmrE: Site-directed spin labeling of transmembrane segment 1. *Biochemistry 42*, 6099−6105.

(20) Pannier, M., Veit, S., Godt, A., Jeschke, G., and Spiess, H. W. (2000) Dead-time free measurement of dipole-dipole interactions between electron spins. *J. Magn. Reson. 142*, 331−340.

(21) Jeschke, G., Chechik, V., and Ionita, P. (2006) DeerAnalysis2006: A comprehensive software package for analyzing pulsed ELDOR data. *Appl. Magn. Reson. 498*, 473−498.

(22) Chiang, Y. W., Borbat, P. P., and Freed, J. H. (2005) The determination of pair distance distributions by pulsed ESR using Tikhonov regularization. *J. Magn. Reson. 172*, 279−295.

(23) Zou, P., and Mchaourab, H. S. (2009) Alternating Access of the Putative Substrate-Binding Chamber in the ABC Transporter MsbA. *J. Mol. Biol. 393*, 574−585.

(24) Le Maire, M., Champeil, P., and Moller, J. V. (2000) Interaction of membrane proteins and lipids with solubilizing detergents. *Biochim. Biophys. Acta 1508*, 86−111.

(25) Polyhach, Y., Bordignon, E., and Jeschke, G. (2011) Rotamer libraries of spin labelled cysteines for protein studies. *Phys. Chem. Chem. Phys. 13*, 2356−2366.

(26) Long, F., Rouquette-Loughlin, C., Shafer, W. M., and Yu, E. W. (2008) Functional cloning and characterization of the multidrug efflux pumps NorM from *Neisseria gonorrhoeae* and YdhE from *Escherichia coli*. *Antimicrob. Agents Chemother. 52*, 3052−3060.

(27) Edgar, R., and Bibi, E. (1997) MdfA, an *Escherichia coli* multidrug resistance protein with an extraordinarily broad spectrum of drug recognition. *J. Bacteriol. 179*, 2274−2280.

(28) Bolhuis, H., Poelarends, G., Van Veen, H. W., Poolman, B., Driessen, A. J., and Konings, W. N. (1995) The lactococcal lmrP gene encodes a proton motive force-dependent drug transporter. *J. Biol. Chem. 270*, 26092−26098.

(29) Gottesman, M. M., and Pastan, I. (1993) Biochemistry of multidrug resistance mediated by the multidrug transporter. *Annu. Rev. Biochem. 62*, 385−427.

(30) Eicher, T., Cha, H., Seeger, M. a., Brandstätter, L., El-Delik, J., Bohnert, J. a., Kern, W. V., Verrey, F., Grütter, M. G., Diederichs, K., and Pos, K. M. (2012) Transport of drugs by the multidrug transporter AcrB involves an access and a deep binding pocket that are separated by a switch-loop. *Proc. Natl. Acad. Sci. U.S.A. 109*, 5687−5692.

(31) Soskine, M., Adam, Y., and Schuldiner, S. (2004) Direct evidence for substrate-induced proton release in detergent-solubilized EmrE, a multidrug transporter. *J. Biol. Chem. 279*, 9951−9955.
(32) Fluman, N., Ryan, C. M., Whitelegge, J. P., and Bibi, E. (2012) Dissection of mechanistic principles of a secondary multidrug efflux protein. *Mol. Cell 47*, 777−787.
(33) Claxton, D. P., Quick, M., Shi, L., De Carvalho, F. D., Weinstein, H., Javitch, J. A., and Mchaourab, H. S. (2010) Ion/substrate-dependent conformational dynamics of a bacterial homolog of neurotransmitter:-sodium symporters. *Nat. Struct. Mol. Biol. 17*, 822−829.
(34) Hänelt, I., Wunnicke, D., Bordignon, E., Steinhoff, H.-J., and Slotboom, D. J. (2013) Conformational heterogeneity of the aspartate transporter Glt(Ph). *Nat. Struct. Mol. Biol. 20*, 210−214.
(35) Georgieva, E. R., Borbat, P. P., Ginter, C., Freed, J. H., and Boudker, O. (2013) Conformational ensemble of the sodium-coupled aspartate transporter. *Nat. Struct. Mol. Biol. 20*, 215−221.